ON THE EFFECT OF CAVITATION ON THE RADIAL FORCES AND HYDRODYNAMIC STIFFNESS OF A CENTRIFUGAL PUMP*

R.J. Franz, C.E. Brennen, A.J. Acosta, and T.K. Caughey
California Institute of Technology
Pasadena, California 91125

The asymmetric flow within a volute exerts a radial force on a centrifugal impeller. The present paper presents experimental measurements of the radial forces on the impeller in the presence of cavitation.

NOMENCLATURE

[A] hydrodynamic force matrix, non-dimensionalized by $\rho\pi\omega^2 r_2^2 b_2$

A_1, A_2 impeller inlet area (πr_1^2), outlet area $(2\pi r_2 b_2)$

b_2 impeller discharge width (0.62 in)

{F} 6-component generalized force vector

F_1, F_2 components of the instantaneous lateral force on the impeller in the rotating dynamometer reference frame

F_x, F_y components of the instantaneous lateral force on the impeller in the fixed laboratory reference frame (X,Y), non-dimensionalized by $\rho\pi\omega^2 r_2^3 b_2$

F_{ox}, F_{oy} values of F_x and F_y if the impeller was located at the the origin of the (X,Y) coordinate system (volute center), non-dimensionalized by $\rho\pi\omega^2 r_2^3 b_2$

* The authors are indebted to the NASA George Marshall Space Flight Center, Alabama for continued sponsorship of this research under contract NAS8-33108. We are also grateful for the help given by D. Brennen.

F_N, F_T — components of the lateral force on the impeller normal to and tangential to the whirl orbit, averaged over the orbit, non-dimensionalized by $\rho\pi\omega^2 r_2^2 b_2 \varepsilon$

$$F_N = (A_{xx} + A_{yy})/2 \quad F_T = (-A_{xy} + A_{yx})/2$$

p_1, p_{t1} — upstream static, total pressure

p_2, p_{t2} — downstream static, total pressure

p_I — static pressure at impeller inlet, $p_{t1} - \rho(\frac{Q}{A_1})^2/2$

p_v — vapor pressure of water

Q — flow rate

r_1, r_2 — impeller inlet, discharge radius (1.594 in., 3.188 in.)

t — time

(X,Y) — fixed laboratory reference frame

x, y — instantaneous coordinates of the impeller center in the fixed laboratory reference frame (X,Y), non-dimensionalized by r_2

ε — radius of the circular whirl orbit

θ — angle of the impeller on the eccentric circle, measured from the volute tongue in the direction of impeller rotation

ρ — density of water

σ — cavitation number, $\dfrac{p_I - p_v}{\rho\omega^2 r_1^2/2}$

ϕ flow coefficient based on the impeller discharge area and tip speed, $\frac{Q}{\omega r_2 A_2}$

ψ total head coefficient, $\frac{p_{t2}-p_{t1}}{\rho\omega^2 r_2^2}$

ω radian frequency of the impeller (shaft) rotation

INTRODUCTION

Earlier papers (refs.1-8) have described measurements of the radial forces and hydrodynamically induced rotordynamic coefficients of centrifugal pumps with various impellers and volutes. All of these earlier measurements were made in the absence of any cavitation within the pump. Yet there is some evidence that the presence of cavitation may have a significant effect on these forces and coefficients. Indeed some tests of the high speed pumps in the Space Shuttle Main Engine have suggested a change in the rotordynamics when cavitation occurs (ref. 9). The present paper is a supplement to our earlier measurements of forces and coefficients and constitutes an exploration of the influence of cavitation.

The references 6-8 provide a complete description of the facility. Briefly, the dynamometer, composed of two parallel plates connected by four strain gaged posts, is mounted between the impeller and the drive shaft. It measures the six components of a generalized hydrodynamic force vector {F} acting on the impeller. The impeller can be subject to whirling motion in an orbit eccentric to the volute center, in addition to the normal impeller rotation. Since the eccentric motion is in the lateral plane, perpendicular to the impeller centerline, only the two components of the force vector {F} in this lateral plane will be discussed.

These forces can be represented by

$$\begin{Bmatrix} F_x \\ F_y \end{Bmatrix} = \begin{Bmatrix} F_{ox} \\ F_{oy} \end{Bmatrix} + [\ A\ ] \begin{Bmatrix} x \\ y \end{Bmatrix} \tag{1}$$

Refering to figure 1, F_x and F_y are in the volute frame of reference, and x and y represent the coordinates of the impeller center measured from the volute center. Dimensionless quantities are used throughout (see Nomenclature for definitions). The present results are only for the case of no whirl: x and y are fixed in time. When the impeller is located at an angular position, θ, on the circular whirl orbit of radius ε, equation (1) is written as

$$\begin{Bmatrix} F_x \\ F_y \end{Bmatrix} = \begin{Bmatrix} F_{ox} \\ F_{oy} \end{Bmatrix} + [\ A\ ] \begin{Bmatrix} \varepsilon/r_2 \cos\theta \\ \varepsilon/r_2 \sin\theta \end{Bmatrix} \tag{2}$$

The steady lateral forces, represented by F_x and F_y, can be considered as the sum of two forces: a fixed force, represented by F_{ox} and F_{oy}, which the impeller would experience if located at the volute center, and a force due to the eccentric displacement of the impeller, represented by a "stiffness" matrix [A]. By taking data at four fixed eccentric positions of the impeller, 90 degrees apart, the matrix [A] and the vector $\{F_o\}$ can be extracted. The gravitational and buoyancy forces on the rotor are subtracted out.

EXPERIMENTS

In references 6-8 results were presented for a typical impeller (impeller X), a five bladed Byron-Jackson centrifugal impeller with a specific speed of 0.57, operating in a spiral volute (volute A) at various impeller speeds ($\lesssim$ 2000 rpm) and flow rates. In order to test under cavitating conditions, the impeller speed was increased to 3000 rpm and the water was substantially de-aerated.

In the following pages the results for three different flow rates are presented: the flow rates chosen are below design (ϕ=0.060), design (ϕ=0.092) and above design (ϕ=0.104). Cavitation performance curves for each of these flow rates are presented in figure 2. We observe that the breakdown cavitation numbers for the three flow rates tested are 0.17, 0.26 and 0.30 respectively.

RESULTS

Results for the radial forces, F_{ox} and F_{oy}, and for the stiffness coefficients are presented in figures 3 through 8. A quick glance will show that large changes occur in both characteristics as the pump approaches and passes through breakdown. Notice that the steady force shown in figures 3 and 4 changes in both magnitude and direction.

Figures 3 and 4 show that for ϕ=0.060 the magnitude of $\{F_o\}$ decreases with performance loss with a small change in direction. For both ϕ=0.092 and ϕ=0.104, the magnitude of $\{F_o\}$ has a minimum with decreasing head coefficent. For each flow coefficient, the direction of $\{F_o\}$ rotates away from the tongue. For ϕ=0.092, $\{F_o\}$ rotates through more than 180° as the pump progresses through breakdown.

Figures 5-8 show the hydrodynamic force matrix [A] from equation (2). These no-whirl results corrrespond to -[K] of the quadratic fit of reference 2 to whirl data for mass, damping and stiffness matrices. The three flow coefficients exhibit the same trends. The diagonal elements decrease with performance loss. The off-diagonal elements first decrease slightly in magnitude with lower cavitation number then increase with performance loss. Figure 8 indicates that the off-diagonal elements do not change monotonically with head coefficient.

In summary, cavitation affects the steady forces, both the impeller-centered force $\{F_o\}$ and the hydrodynamic force matrix [A], exerted upon an eccentric impeller. It is useful to interprete the matrix [A] in terms of the average normal force, F_N, and the tangential force, F_T, acting on a whirling impeller in the limit as the whirl speed approaches zero. With cavitation breakdown, the normal force is reduced while the tangential force is increased. Further tests are planned to examine the unsteady flow effects which occur at non-zero whirl speed. More specifically, the frequency dependence in the matrix [A] (the damping and added mass components) will shortly be examined as a function of cavitation number.

REFERENCES

1. Agostinelli, A., Nobles, D., and Mockridge, C. R., "An Experimental Investigation of Radial Thrust in Centrifugal Pumps", ASME Journal of Engineering for Power, Vol. 82, pp. 120-126, April 1960.

2. Domm, H., and Hergt, P., "Radial Forces on Impeller of Volute Casing Pumps", Flow Research on Blading (L. S. Dzung, ed.), Elsevier Pub. Co., The Netherlands, pp 305-321, 1970.

3. Ohashi, H. and Shoji, H., "Lateral Fluid Forces Acting on a Whirling Centrifugal Impeller in Vaneless and Vaned Diffuser," Third Workshop on Rotordynamic Instability Problems in High-Performance Turbomachinery, Texas A&M University, May 28-30, 1984.

4. Chamieh, D. S., "Forces on a Whirling Centrifugal Pump-Impeller", Ph. D. Thesis, Division of Engineering and Applied Science, California Institute of Technology, February 1983.

5. Chamieh, D. S., Acosta, A. J., Brennen, C. E. and Caughey, T. K., "Experimental Measurements of Hydrodynamic Radial Forces and Stiffness Matrices for a Centrifugal Pump-Impeller," ASME Journal of Fluids Engineering, Vol. 107, Sept. 1985, pp. 307-315.

6. Jery, B., Acosta, A.J., Brennen, C.E., and Caughey, T.K., "Hydrodynamic Impeller Stiffness, Damping and Inertia in the Rotordynamics of Centrifugal Pumps," "Third Workshop on Rotordynamic Instability Problems in High Performance Turbomachinery", Texas A&M University, May 28-30,1984.

7. Jery, B., Brennen, C.E., Caughey, T.K., and Acosta, A.J., "Forces on Centrifugal Pump Impellers," "Second International Pump Symposium", Houston, Texas, April 29-May 2,1985.

8. Jery, B., "Experimental Study of Unsteady Hydrodynamic Force Matrices on Whirling Centrifugal Pump-Impellers", Ph. D. Thesis, Division of Engineering and Applied Science, California Institute of Technology, October 1985.

9. Rocketdyne Division, Rockwell, personal communication

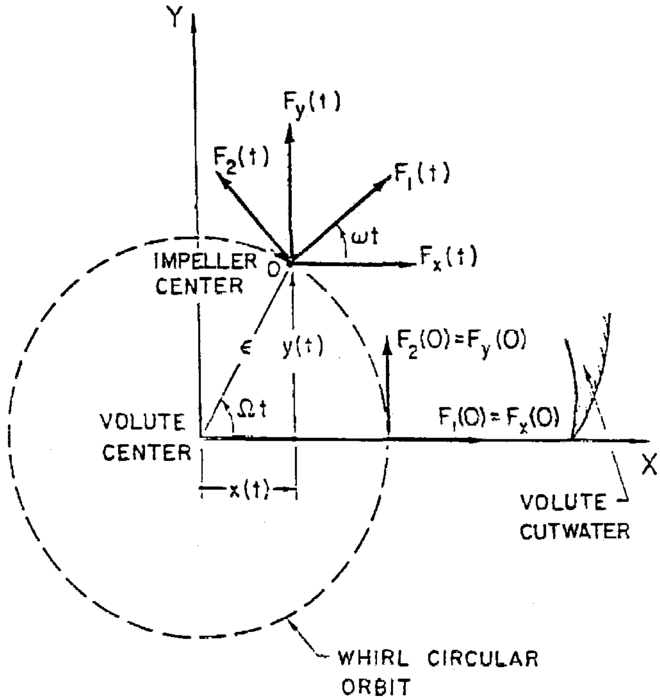

Figure 1 Schematic representation of the position of the impeller within the volute. The measured forces are indicated in the rotating dynamometer frame (as F_1, F_2) and in the stationary volute frame (as F_x, F_y).

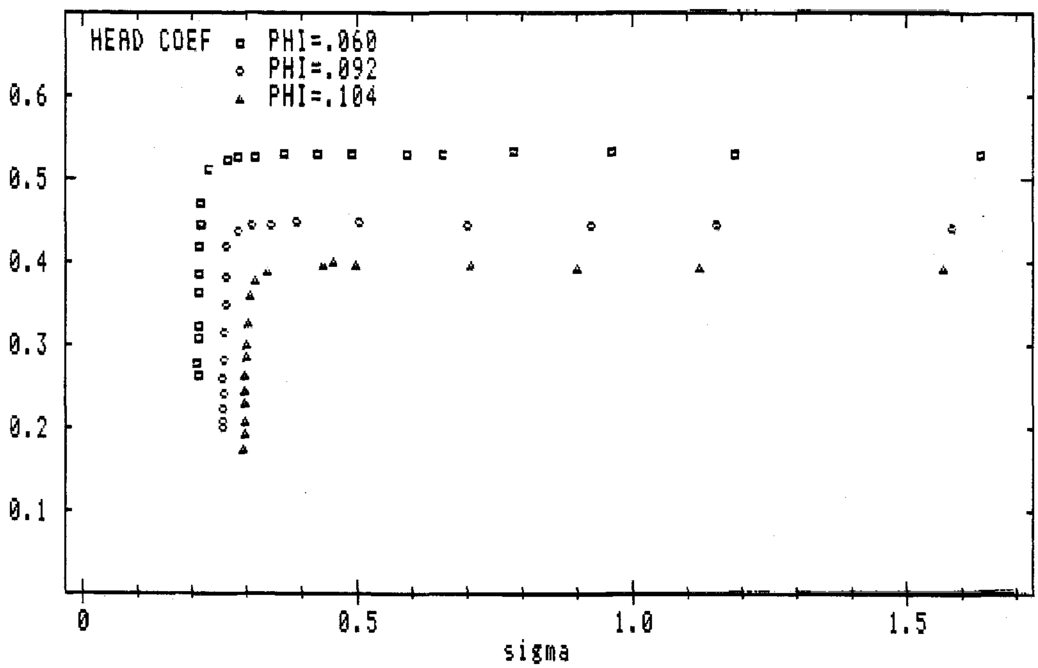

Figure 2 Cavitation performance curves for the three flow coefficients: ϕ=0.060 (below design), ϕ=0.092 (design) and ϕ=0.104 (above design), for volute A/impeller X at 3000 rpm.

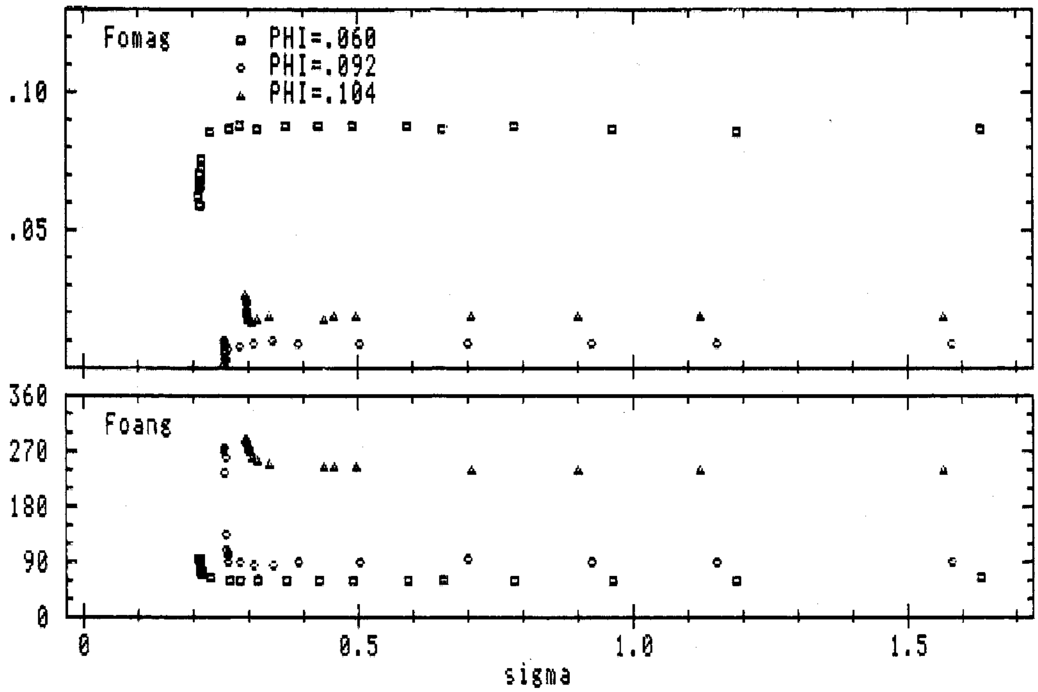

Figure 3 The dependence of the magnitude and direction of the volute force, $\{F_o\}$, on cavitation number for the three flow coefficients: ϕ=0.060, ϕ=0.092, ϕ=0.104, for volute A/impeller X at 3000 rpm.

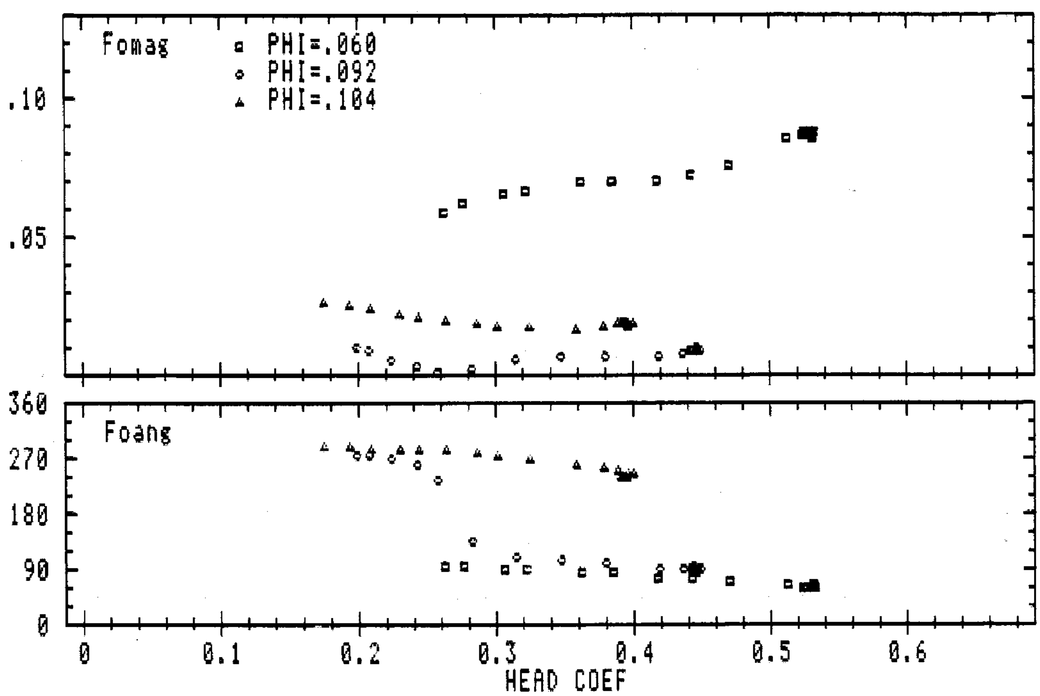

Figure 4 The dependence of the magnitude and direction of the volute force, $\{F_o\}$, on head coefficient for the three flow coefficients: ϕ=0.060, ϕ=0.092, ϕ=0.104, for volute A/impeller X at 3000 rpm.

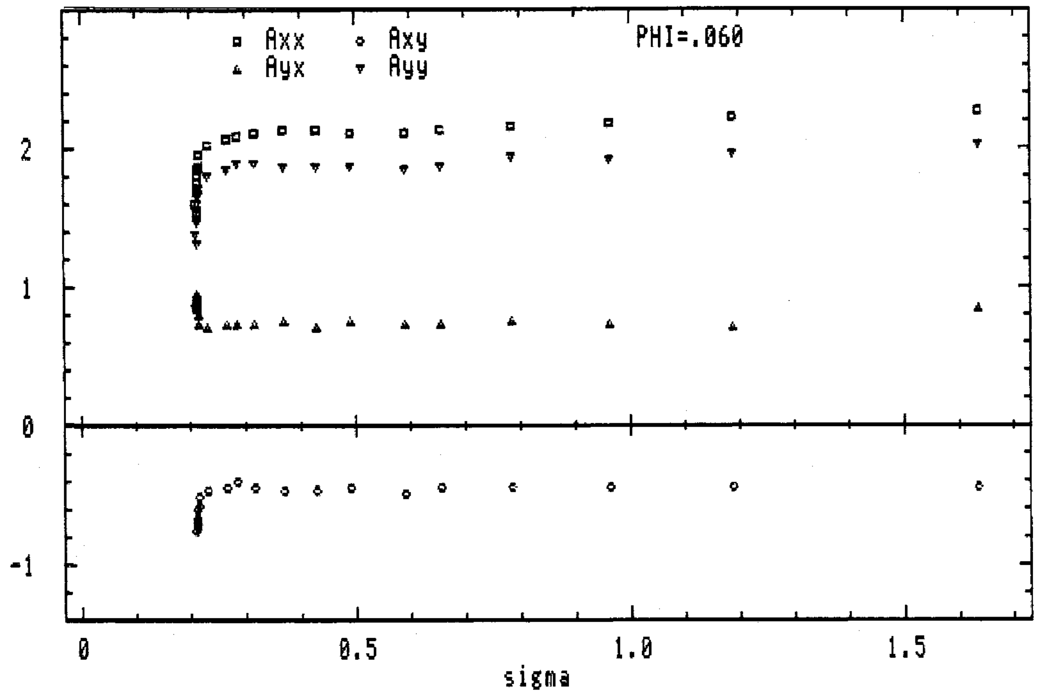

Figure 5 The dependence of the elements of the hydrodynamic force matrix, [A], on cavitation number for ϕ=0.060 (below design), for volute A/impeller X at 3000 rpm.

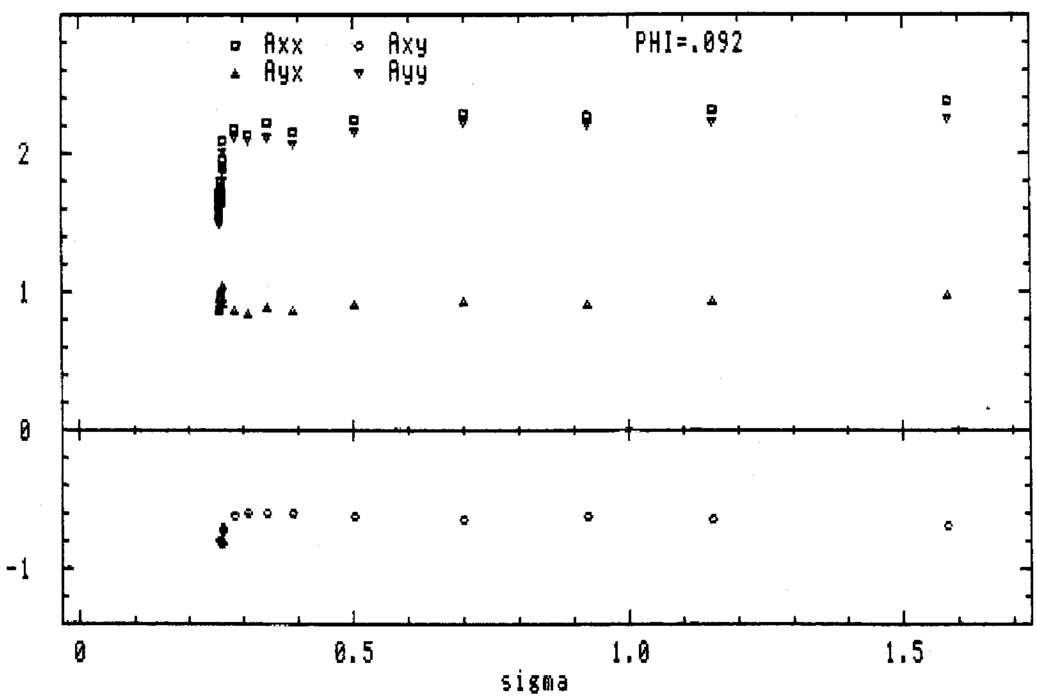

Figure 6 The dependence of the elements of the hydrodynamic force matrix, [A], on cavitation number for ϕ=0.092 (at design), for volute A/impeller X at 3000 rpm.

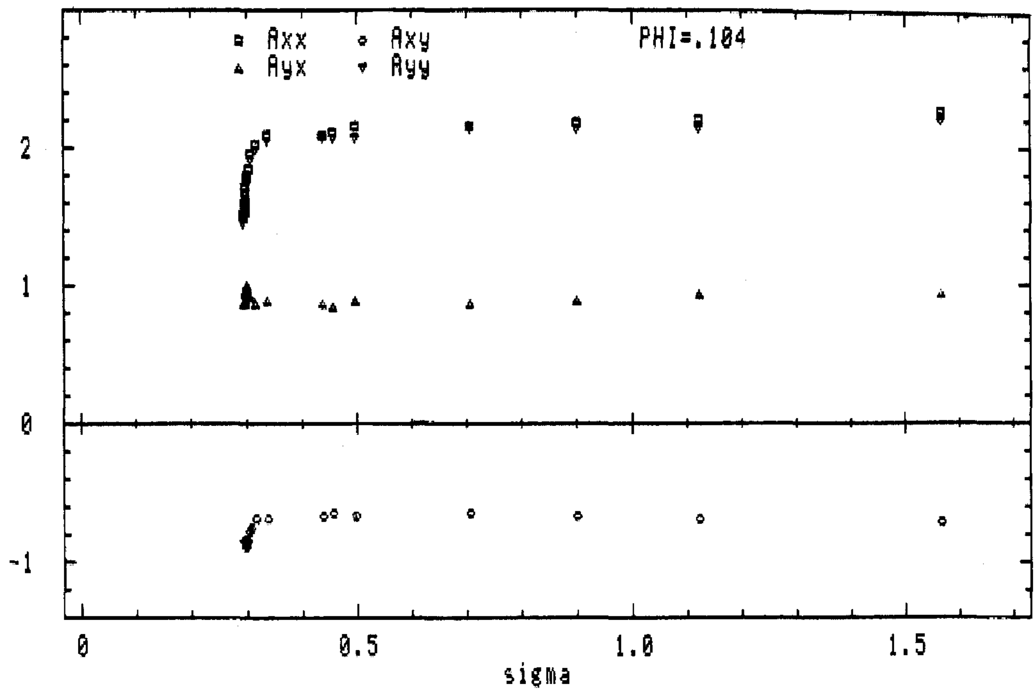

Figure 7 The dependence of the elements of the hydrodynamic force matrix, [A], on cavitation number for ϕ=0.104 (above design), for volute A/impeller X at 3000 rpm.

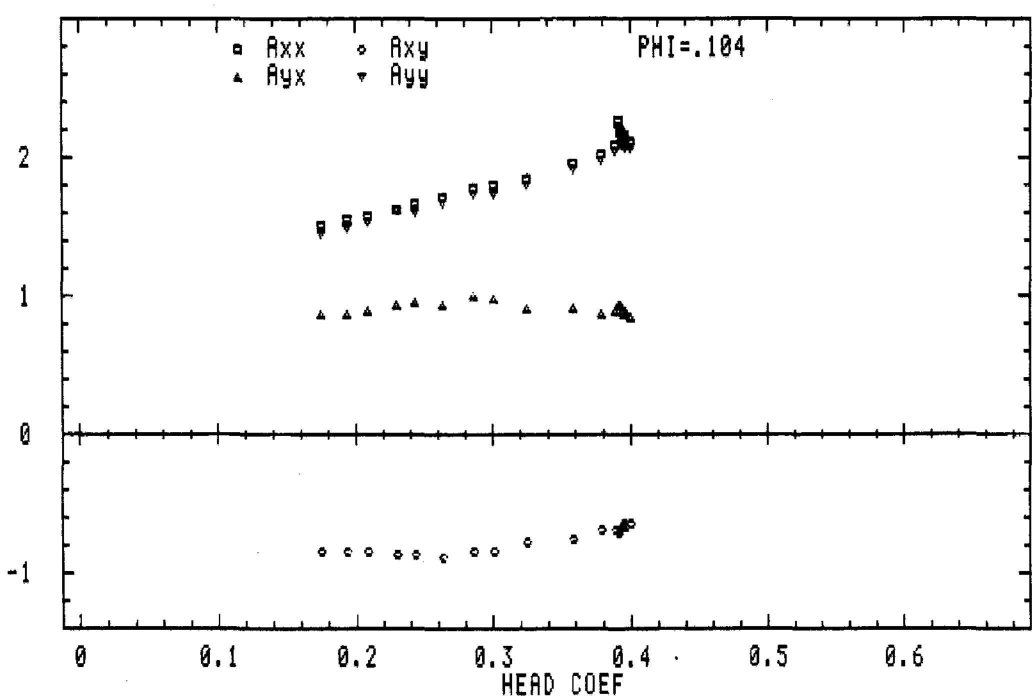

Figure 8 The dependence of the elements of the hydrodynamic force matrix, [A], on head coefficient for ϕ=0.104 (above design), for volute A/impeller X at 3000 rpm.